Hue University Journal of Science: Natural Science
Vol. 135, No. 1B, 5–24, 2026

pISSN 1859-1388
eISSN 2615-9678

Chemical composition of *Homalomena occulta* essential oil and molecular docking–admet evaluation against antimicrobial targets

Nguyen Vinh Phu[1], Tran Hoang Ha[2], Nguyen Tran Thien Phu[3], Nguyen Vu Bao Ngoc[3], Tran Quang Huy[2], Nguyen Dai Chau[2], Nguyen Thi Thanh Hai[2], Phan Tu Quy[4], Tran Nhat Phong Dao[5], Nguyen Thi Ai Nhung[2]*

[1] Faculty of Basic Sciences, University of Medicine and Pharmacy, Hue University, Hue, Viet Nam
[2] Department of Chemistry, University of Sciences, Hue University, Hue, Viet Nam
[3] HUSC High School for Gifted Students, Hue, Viet Nam
[4] Department of Natural Sciences & Technology, Tay Nguyen University, Buon Ma Thuot, Viet Nam
[5] Faculty of Traditional Medicine, Can Tho University of Medicine and Pharmacy, Can Tho, Viet Nam

* Correspondence to Nguyen Thi Ai Nhung <ntanhung@hueuni.edu.vn>

(*Received: 26 January 2026; Revised: 11 February 2026; Accepted: 11 February 2026*)

Abstract. *Homalomena occulta (H. occulta)* essential oil was obtained via steam distillation, and its chemical composition was characterized using gas chromatography–mass spectrometry (GC–MS) analysis. A total of 43 compounds were identified predominantly oxygenated monoterpenes, with linalool (40.35%), terpinen-4-ol (8.54%), and α-terpineol (3.05%) as the most abundant components. The identified compounds were evaluated *in silico* through molecular docking simulations using MOE 2022.10 software against three antimicrobial-related targets associated with pathogenic strains, namely, *Streptococcus pyogenes* (P0C0C7), *Streptococcus pneumoniae* (Q8DQF8), and *Candida albicans* (4ESW). Several promising candidates with the strongest predicted inhibitory potential were identified and ranked for each target as follows: P0C0C7: **40** (-11.2 kcal.mol^{-1}) > **27** (-11.0 kcal.mol^{-1}) > **4** (-10.9 kcal.mol^{-1}) ≈ **36** (-10.9 kcal.mol^{-1}) > **29** (-10.4 kcal.mol^{-1}); Q8DQF8: **27** (-9.6 kcal.mol^{-1}) > **29** (-9.4 kcal.mol^{-1}) > **25** (-9.3 kcal.mol^{-1}) ≈ **41** (-9.3 kcal.mol^{-1}) > **36** (-9.2 kcal.mol^{-1}) and 4ESW **42** (-11.3 kcal.mol^{-1}) > **38** (-10.8 kcal.mol^{-1}) > **21** (-10.7 kcal.mol^{-1}) > **32** (-10.3 kcal.mol^{-1}) ≈ **41** (-10.3 kcal.mol^{-1}). A drug-likeness study based on Lipinski's rule of five was generally favorable (MW < 500 Da for 43/43 compounds; logP < 5 for 41/43 compounds). The ADMET prediction results suggested good absorption and permeability, along with a low risk of major transporter- and metabolism-related issues. Overall, these findings provide a strong *in silico* basis supporting further experimental antimicrobial testing for *H. occulta* essential oil.

Keywords: *Homalomena occulta*, P0C0C7, Q8DQF8, 4ESW, molecular docking, ADMET

1 Introduction

Microbial diseases—particularly respiratory bacterial infections and superficial cutaneous mycoses—remain a significant public health burden worldwide [1,2]. The prolonged and inappropriate use and misuse of antibiotics, antivirals, and antifungal drugs have contributed to the emergence and spread the growth of drug-resistant strains, leading to reduced therapeutic efficacy, increasing healthcare costs, and a higher incidence of adverse effects [3]. In addition, the indiscriminate use of antibacterial and antifungal agents increases selection pressure for resistant strains and can cause dose-limiting side effects, including disruption of the gut microbiota, hypersensitivity reactions, and hepatic and renal toxicity [4]. In the context of the continual emergence of new pathogens, the need of

identification of safe and sustainable antimicrobial agents has become increasingly urgent.

In recent years, natural compounds derived from medicinal plants, particularly plant essential oils, have received increasing attention as potential agents for controlling pathogenic microorganisms [5]. Owing to their rich content of many biologically active components, essential oils can inhibit microbial growth through various mechanisms, including membrane disruption of cell membrane structure and permeability [6], inhibition of key enzymatic activities, and interference with biofilm formation [7]. The diversity of their chemical compositions, combined with their multitarget modes of action, make plant essential oils promising sources of raw materials for the development of therapeutic products that support the treatment of bacterial and fungal infections while simultaneously reducing the risk of antimicrobial resistance development [8, 9].

H. occulta is a medicinal plant that has been traditionally used in Vietnamese folk medicine, particularly in central Vietnam, with reported effects such as pain relief, anti-inflammatory effects, improved blood circulation, and support for the treatment of certain skin diseases [10,11]. Preliminary studies indicate that *H. occulta* contains bioactive compounds capable of inhibiting microbial growth, particularly pathogenic bacteria and fungi associated with skin infections and respiratory diseases [12]. Another study reported that the essential oil of *H. occulta* exhibits antibacterial, anti-inflammatory, and antioxidant activities [10], but comprehensive data regarding its mechanism of action, efficacy, formulation studies, and practical applications remain limited.

In terms of the increasing burden of respiratory and cutaneous infections [13, 14] and the concurrent challenge posed by antimicrobial resistance [2], investigating the pathogens implicated in these conditions is of critical importance. Among the organisms of particular interest, *Streptococcus pyogenes*, *Streptococcus pneumoniae*, and *Candida albicans*, which are frequently selected in mechanistic studies to clarify pathogenic pathways and to inform effective control and therapeutic strategies, have been consistently recognized as high-priority targets.

S. pyogenes and *S. pneumoniae* are Gram-positive bacteria that commonly colonize the oropharyngeal region, where they can cause pharyngitis and pneumonia and, if not adequately controlled, lead to severe complications [15,16]. For *S. pyogenes*, LuxS was selected as the target enzyme because it is responsible for AI-2 signal production, thereby contributing to quorum sensing and biofilm formation [17]; its experimentally determined structure is available in UniProtKB under accession P0C0C7 (LUXS_STRPY). *S. pneumoniae* possesses an ATP-binding protein of the ABC transporter system, which is involved in the efflux of toxic compounds and antibiotics, thereby contributing to bacterial adaptation and antimicrobial resistance [18]; the structure of this protein has been characterized and is available in the UniProtKB database under accession Q8DQF8 (Q8DQF8_STRR6).

C. albicans is a prevalent yeast responsible for a broad disease spectrum, ranging from mucosal candidiasis (e.g., vulvovaginitis and oral thrush) to skin–nail involvement and invasive infections such as pneumonia and urinary tract infections [19]. THI5p was selected as the target enzyme because it plays an essential role in thiamine biosynthesis, directly impacts fungal growth and viability, and therefore represents a promising target for developing inhibitory strategies against *C. albicans* [20]. The crystal

pISSN 1859-1388
eISSN 2615-9678

structure of THI5p has been resolved and deposited in the Protein Data Bank under PDB ID 4ESW (DOI: https://doi.org/10.2210/pdb4ESW/pdb).

In this study, *H. occulta* essential oil was extracted, and its chemical composition was characterized via GC–MS analysis. The antibacterial and antifungal potential of the oil was then evaluated *in silico* against three protein targets, namely, P0C0C7, Q8DQF8, and 4ESW, corresponding to *S. pyogenes*, *S. pneumoniae*, and *C. albicans*, respectively. The docking results were interpreted on the basis of binding energies as well as the principal chemical interactions observed within the docking processes. Moreover, drug likeness and safety were assessed via Lipinski-based descriptors and ADMET prediction tools to provide early insights into developability. Overall, these findings support the antimicrobial potential of *H. occulta* essential oil and provide a rationale for further experimental validation.

2 Methods

2.1 Experiment

Plant material

H. occulta was collected in 2024-2025 (Fig. 1) from Loc An commune, Hue City, Viet Nam. The plant material was taxonomically identified by comparison with reference descriptions by Msc. Nguyen Dai Chau and stored at the Institute for Research and Application of Science and Technology, University of Sciences, Hue University.

Fig. 1. Morphological characteristics of *H. occulta* (whole plant showing leaves, rhizomes, and roots)

Essential oil extraction

The essential oils from the leaves of *H. occulta* were extracted by steam distillation. Briefly, 30 kg of coarsely ground raw material was subjected to distillation with approximately 50 L of water. The resulting crude essential oil, which remained partially saturated with water, was dried over anhydrous sodium sulfate to obtain the purified oil.

Identification of *H. occulta* essential oil

The chemical composition of *H. occulta* essential oil was analyzed using gas chromatography–mass spectrometry (GC–MS) on an Agilent 7890B system interfaced with a 5975C mass-selective detector. The separation employed an HP-5MS fused silica capillary column (30 m × 250 μm × 0.25 μm). Chromatographic and mass spectral data were acquired and processed via software integrated with the GC–MS system. Individual components of the essential oil were identified on the basis of their retention times (RTs) and by comparing their mass spectra with those in a standard reference library (NIST14), with a similarity threshold set at ≥ 85%.

2.2 Computation

Computational input preparation

The crystal structures of the selected bacterial target proteins from *S. pyogenes* (P0C0C7) and *S. pneumoniae* (Q8DQF8), together with the reference

antibacterial drug penicillin G (**D1**), are shown in Fig. 2. Similarly, the crystal structure of the target protein from *C. albicans* (4ESW), along with the reference antifungal agent clotrimazole (**D2**), is presented in Fig. 3.

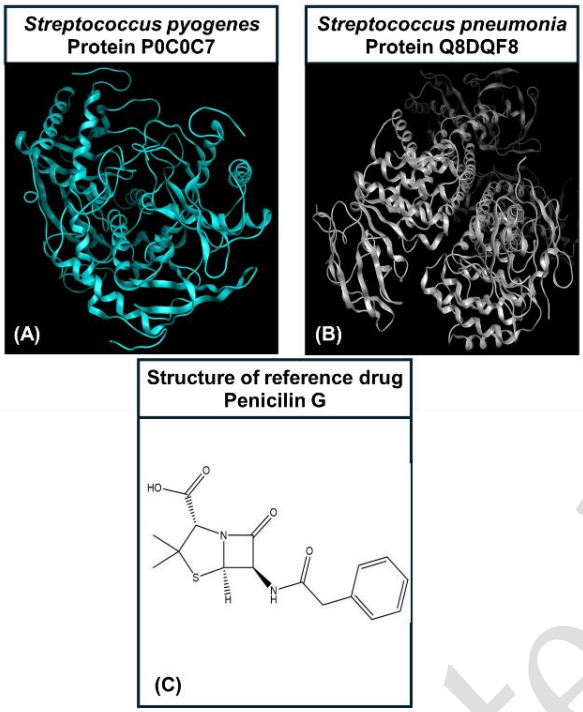

Fig. 2. Structures of the target proteins (A) P0C0C7 and (B) Q8DQF8; (C) structure of the reference drug penicillin G

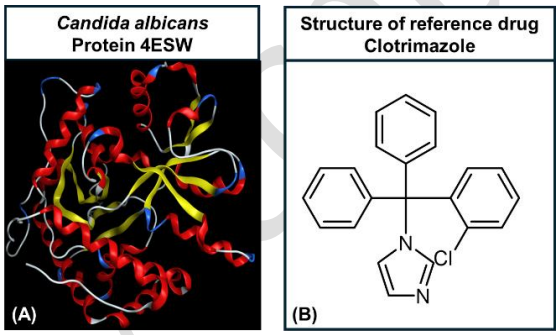

Fig. 3. Structures of the target proteins (A) 4ESW and (B) the reference drug clotrimazole

Molecular docking simulation

Molecular docking was utilized to predict the binding energies and interaction modes between the investigated natural compounds and target proteins and to evaluate their potential antibacterial activity using MOE 2022.10 software. The molecular docking workflow was conducted following a five-step procedure as previously reported [21–23].

Step 1. Protein preparation: Target proteins were selected from appropriate protein libraries or databases. The protein structure was prepared by removing water molecules and unnecessary polymer chains. The binding site was defined on the basis of the position of the cocrystallized ligand.

Step 2. Ligand preparation: For ligand preparation, the 2D chemical structures of the investigated compounds were first drawn and automatically converted into 3D conformations via ChemBioOffice 2018, after which the resulting 3D geometries were energy-minimized in SYBYL-X 1.1. This process was automatically repeated five times to generate multiple conformations, followed by final energy minimization to obtain optimized molecular structures suitable for subsequent docking studies.

Step 3. Molecular docking: Molecular docking simulations were performed via MOE 2022.10, which uses the triangle matching placement method to position ligand fragments within the binding pocket, with a maximum of 1000 poses generated per iteration and up to 200 poses retained per ligand fragment. The most favorable ligand binding poses were identified by the minimum docking score (DS, kcal.mol^{-1})

Step 4. Redocking: The reliability of the docking parameters was validated through a redocking procedure via three distinct workflows: (i) extraction of the ligand from the cocrystalline protein–ligand complex; (ii) re-preparation of the ligand according to Step 1; and (iii) redocking of the ligand. The docking simulation was considered reliable when the root-mean-square deviation (RMSD) was < 2.0 Å, which reflects the deviation between the original crystallographic

pISSN 1859-1388
eISSN 2615-9678

backbone conformation (after Step 3) and the redocked pose (after Step 4).

Step 5. Analysis results: The inhibitory potential of the investigated compounds toward the target proteins was evaluated on the basis of the docking score (DS, kcal.mol^{-1}) and the RMSD values. In addition, ligand–target interactions were analyzed and visualized in both 2D and 3D representations, including hydrogen bonds, π–π interactions, ionic interactions, and cation–π interactions, whereas van der Waals surface contacts were identified through hydrophobic and steric surface complementarity between the compounds and the amino acids of the target proteins.

Physicochemical property analysis

The drug-likeness properties of the candidates were evaluated *in silico* according to Lipinski's Rule of Five [24]. Key physicochemical descriptors, including molecular weight (MW), molecular volume, and lipophilicity/solubility indices (logP and logS), were computed via ADMETlab 3.0, whereas molecular polarizability was derived via ChemDoodle Web. The compounds were prioritized if they exhibited favorable membrane permeability profiles adhering to the established thresholds: MW ≤ 500 Da, logP ≤ 5, HBA ≤ 10, and HBD ≤ 5.

2.2.1 ADMET prediction

The pharmacokinetic-toxicity properties of the investigated compounds—encompassing absorption, distribution, metabolism, excretion, and toxicity (ADMET)—were predicted via the SwissADME platform developed and maintained by the Swiss Institute of Bioinformatics, whereas the theoretical assessment was conducted in accordance with the framework (http://biosig.unimelb.edu.au/pkcsm/theory) proposed by Pires and coworkers [25] and supported through collaboration between the University of Melbourne and the University of Cambridge. These pharmacokinetic-toxicity parameters serve as decisive criteria for assessing drug-likeness and developability, thereby supporting the prioritization of candidates for further therapeutic investigation.

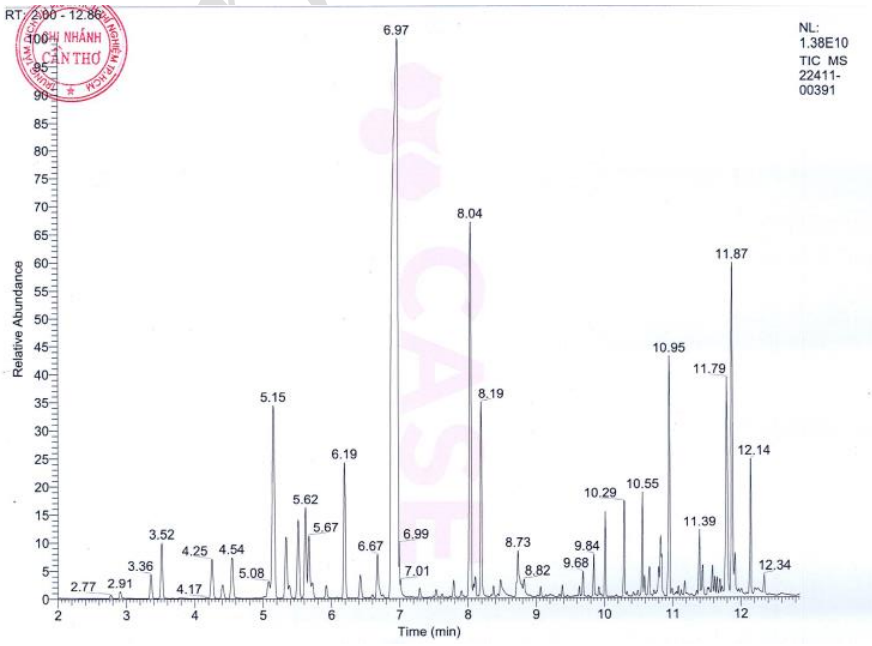

Fig. 4. Gas chromatography spectrum of *H. occulta* essential oil

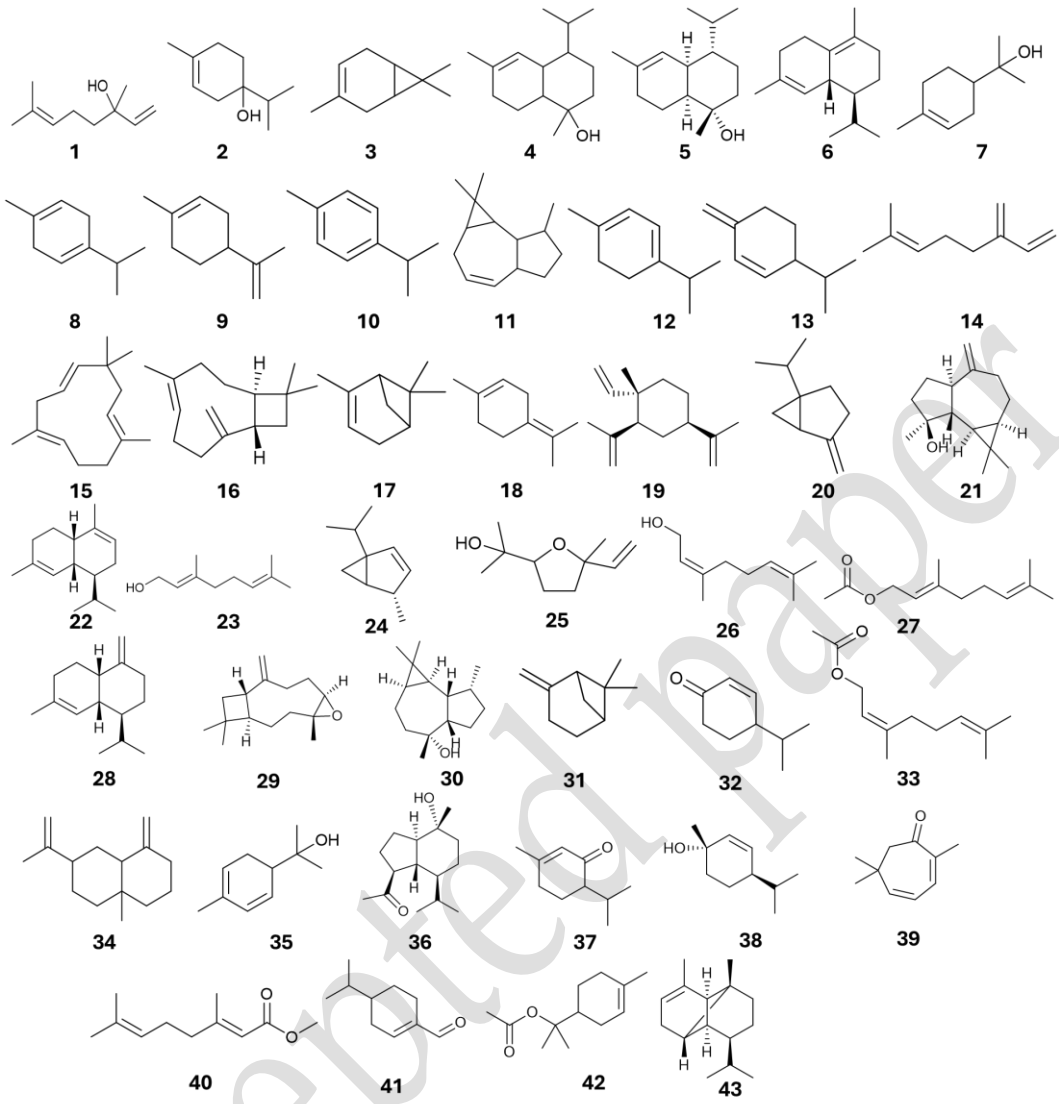

Fig. 5. Chemical structures of the investigated compounds (**1-43**) from *H. occulta* essential oil

Table 1. Identification of major bioactive compounds in *H. occulta* essential oil.

Compound	Formula	Retention time (min)	Percentage (%)	Notation
Linalool	$C_{10}H_{18}O$	6.97	40.35	**1**
Terpinen-4-ol	$C_{10}H_{18}O$	8.04	8.54	**2**
3-Carene	$C_{10}H_{16}$	5.15	6.29	**3**
α-Cadinol	$C_{15}H_{26}O$	11.87	5.30	**4**
α-epi-Muurolol	$C_{15}H_{26}O$	11.79	4.43	**5**
Cadina-1(10),4-diene	$C_{15}H_{24}$	10.95	3.60	**6**
α-Terpineol	$C_{10}H_{18}O$	8.19	3.05	**7**
γ-Terpinene	$C_{10}H_{16}$	6.19	2.80	**8**
D-Limonene	$C_{10}H_{16}$	5.62	2.07	**9**

pISSN 1859-1388
eISSN 2615-9678

Compound	Formula	Retention time (min)	Percentage (%)	Notation
p-Cymene	$C_{10}H_{14}$	5.51	1.90	**10**
Isoaromadendrene	$C_{15}H_{24}$	12.14	1.81	**11**
α-Terpinene	$C_{10}H_{16}$	5.34	1.58	**12**
β-Phellandrene	$C_{10}H_{16}$	5.67	1.53	**13**
β-Myrcene	$C_{10}H_{16}$	4.54	1.28	**14**
Humulene	$C_{15}H_{24}$	10.55	1.28	**15**
Caryophyllene	$C_{15}H_{24}$	10.29	1.24	**16**
α-Pinene	$C_{10}H_{16}$	3.52	1.22	**17**
Terpinolene	$C_{10}H_{16}$	6.67	1.06	**18**
β-Elemene	$C_{15}H_{24}$	10.01	1.04	**19**
Sabinene	$C_{10}H16$	4.25	1.03	**20**
Spathulenol	$C_{15}H_{26}O$	11.39	0.90	**21**
α-Muurolene	$C_{15}H_{24}$	10.82	0.83	**22**
Geraniol	$C_{10}H_{18}O$	8.73	0.60	**23**
2-Thujene	$C_{10}H_{16}$	3.36	0.53	**24**
cis-Linalool oxide	$C_{10}H_{18}O_2$	6.42	0.53	**25**
Nerol	$C_{10}H_{18}O$	8.48	0.53	**26**
Geranyl acetate	$C_{12}H_{20}O_2$	9.84	0.51	**27**
γ-Muurolene	$C_{15}H_{24}$	10.66	0.50	**28**
Caryophyllene oxide	$C_{15}H_{24}O$	11.44	0.38	**29**
Ledol	$C_{15}H_{26}O$	11.58	0.37	**30**
β-Pinene	$C_{10}H_{16}$	4.41	0.36	**31**
Cryptone	$C_9H_{14}O$	8.11	0.30	**32**
Nerol acetate	$C_{12}H_{20}O_2$	9.68	0.29	**33**
Eudesma-4(14).11-diene	$C_{15}H_{24}$	10.8	0.29	**34**
α-Phellandrene-8-ol	$C_{10}H_{16}O$	7.79	0.28	**35**
Oplopanone	$C_{15}H_{24}O_2$	12.34	0.28	**36**
p-Menth-1-en-3-one	$C_{10}H_{16}O$	8.82	0.27	**37**
p-Menth-2-en-1-ol	$C_{10}H_{18}O$	7.29	0.17	**38**
Eucarvone	$C_{10}H_{14}O$	8.37	0.17	**39**
Methyl geranate	$C_{11}H_{18}O_2$	9.38	0.16	**40**
Phellandral	$C_{10}H_{16}O$	9.06	0.14	**41**
α-Terpinyl acetate	$C_{12}H_{20}O_2$	9.63	0.12	**42**
Copaene	$C_{15}H_{24}$	9.92	0.12	**43**

3 Results

3.1 Chemical composition

GC–MS analysis of *H. occulta* essential oil (Fig. 4) provided detailed information on its chemical composition, leading to the identification of 43 compounds. The GC–MS results are summarized in Table 1, where the identified compounds are listed in descending order of their percentage. In addition, the corresponding chemical structures of the major constituents are presented in Fig. 5. The results revealed that the chemical composition of *H. occulta* essential oil consists of multiple classes of compounds, predominantly monoterpenes (hydrocarbon and oxygenated) and sesquiterpenes (hydrocarbon and oxygenated), with varying contents among individual constituents. Oxygenated monoterpenes were the most abundant group, with linalool (**1**; 40.35%) being the major compound, followed by terpinen-4-ol (**2**; 8.54%) and α-terpineol (**7**; 3.05%). Other compounds found in lower amounts included geraniol (**23**; 0.60%), nerol (**26**; 0.53%), cis-linalool oxide (**25**; 0.53%), and geranyl acetate (**27**; 0.51%). In the monoterpene hydrocarbon group, the main components were 3-carene (**3**; 6.29%), γ-terpinene (**8**; 2.80%), D-limonene (**9**; 2.07%), and p-cymene (**10**; 1.90%). This group also contained α-terpinene (**12**; 1.58%), β-phellandrene (**13**; 1.53%), β-myrcene (**14**; 1.28%), α-pinene (**17**; 1.22%), terpinolene (**18**; 1.06%), and sabinene (**20**; 1.03%). For sesquiterpene hydrocarbons, the profile was characterized by cadina-1(10),4-diene (**6**; 3.60%), isoaromadendrene (**11**; 1.81%), humulene (**15**; 1.28%), caryophyllene (**16**; 1.24%), and β-elemene (**19**; 1.04%), along with smaller amounts of α-muurolene (**22**; 0.83%) and γ-muurolene (**28**; 0.50%). Finally, the oxygenated sesquiterpenes included α-cadinol (**4**; 5.30%) and α-epi-muurolol (**5**; 4.43%), as well as spathulenol (**21**; 0.90%), caryophyllene oxide (**29**; 0.38%), and ledol (**30**; 0.37%).

3.2 Computational results

Protein inhibitability

Molecular docking was employed to simulate and predict the interactions between 43 compounds identified in *H. occulta* essential oil and the reference drugs with three target proteins, namely, P0C0C7 (*S. pyogenes*), Q8DQF8 (*S. pneumoniae*) and 4ESW (*C. albicans*). Through these simulations, the inhibitory potential of the compounds was evaluated on the basis of key parameters such as the docking score (DS) and root-mean-square deviation (RMSD). In addition, other important interactions, including hydrogen bonding and van der Waals interactions between the investigated compounds and the target proteins, were analyzed in detail. The inhibitory ability of the compounds was evaluated on the basis of two main criteria: the docking score (DS, $kcal.mol^{-1}$) and the number of interactions formed with the target protein with a more negative DS and a higher interaction count generally indicating stronger inhibition. The detailed bonding parameters, including DS ($kcal.mol^{-1}$), RMSD, hydrogen bonding (HB), and van der Waals interactions (VdW), are summarized in Tables S1–S3 for the ligand–P0C0C7, ligand–Q8DQF8, and ligand–4ESW complexes, respectively, and the corresponding poses/interaction maps are shown in Figures S1–S2, S3–S4, and S5–S6 (Supporting Information).

Accordingly, this section discusses the predicted inhibitory binding of the investigated compounds and the reference drug penicillin G (**D1**) to the *S. pyogenes* P0C0C7 target protein. An overall comparison of DS and the numbers of hydrogen bonds and van der Waals interactions is presented in Fig. 6. The docking results revealed a broad range of docking scores (-11.2 to -6.2 $kcal.mol^{-1}$), involving 1–4 hydrogen bonds and 9-16 van der Waals interactions. Several promising candidates with the strongest inhibitory ability

pISSN 1859-1388
eISSN 2615-9678

were identified and can be ranked as **40–P0C0C7** (-11.2 kcal.mol^{-1}) > **27–P0C0C7** (-11.0 kcal.mol^{-1}) > **4–P0C0C7** (-10.9 kcal.mol^{-1}) ≈ **36–P0C0C7** (-10.9 kcal.mol^{-1}) > **29–P0C0C7** (-10.4 kcal.mol^{-1}) (highlight in bold). The corresponding docking details are summarized in Table 2, and visualizations of the docking process are shown in Fig. 7. Compared with the reference drug **D1** (DS = -10.8 kcal.mol^{-1}, HB = 3, VdW = 10), four of the top five compounds (**40**, **27**, **4**, and **36**) presented more favorable DS values than **D1** did. In contrast, compound **3** was the weakest predicted inhibitor of P0C0C7 (**DS = -6.2** kcal.mol^{-1}), showing the lowest predicted binding strength among all the screened ligands under the current docking conditions. In addition, the other compounds had a DS range of approximately -6.9–9.5 kcal.mol^{-1}, which was characterized by the formation of 1–2 hydrogen bonds and 9–16 van der Waals interactions. Although their DS values were lower than those of the top-ranked ligands, several compounds, such as **41–P0C0C7** (-10.3 kcal.mol^{-1}) and **37–P0C0C7** (-10.1 kcal.mol^{-1}), still exhibited relatively strong inhibitory abilities toward protein P0C0C7.

Table 2. Molecular docking simulation results of the ligand–P0C0C7 complexes for the strongest predicted inhibitors

Ligand–protein			Hydrogen bond						van der Waals interaction
Name	**DS**	**Name**	**L**	**P**		**T**	**D**	**E**	
4–P0C0C7	-10.9	0.82	O	O	Glu 60	H-donor	3.17	-0.5	Ser 126, Cys 127, Gly 128, Cys 82, His 14, Asp 40, Leu 12, Arg 23, Phe 80, Arg 42, Ile 25, Asp 76
			O	N	His 57	H-acceptor	3.09	-1.8	
			O	N	His 61	H-acceptor	2.99	-3.2	
27–P0C0C7	-11.0	1.07	O	N	His 57	H-acceptor	3.36	-1.4	His 57, Arg 42, His 14, Cys 127, Cys 82, Ser 126, Arg 23, Cys 77, Ala 64, Asp 76, Ser 78
			O	N	His 61	H-acceptor	3.38	-0.5	
			O	N	Gly 128	H-acceptor	3.25	-0.9	
			C	6-ring	Phe 80	H-π	3.70	-0.5	
29–P0C0C7	-10.4	1.50	O	N	His 57	H-acceptor	3.23	-1.7	Leu 12, Arg 42, His 87, Asp 76, Asp 40, His 14, His 61, Glu 60, Phe 80, Cys 82, Ser 126, Ser 78, Cys 127
			O	N	Gly 128	H-acceptor	3.29	-1.4	
36–P0C0C7	-10.9	1.44	O	N	His 57	H-acceptor	3.20	-0.9	Glu 60, Cys 82, Cys 127, Gly 121, Pro 120, Ser 126, His 14, Leu 12, Asp 40, Ile 25, Phe 80, Arg 42, Arg 23
			O	N	His 61	H-acceptor	2.85	-1.5	
			O	N	Gly 128	H-acceptor	3.08	-1.9	
40–P0C0C7	-11.2	1.18	O	N	His 61	H-acceptor	2.99	-1.1	His 57, Cys 127, Asp 40, Cys 82, Arg 42, Phe 80, Ile 25, His 87, Asp 76, Cys 77, Pro 120, His 14, Gly 121, Ser 126, Glu 60
			O	N	Gly 128	H-acceptor	3.07	-1.4	
			C	5-ring	His 61	H-π	4.31	-0.9	
D1–P0C0C7	-10.8	1.13	S	C	Ser 99	H-acceptor	3.51	-0.7	Lys 15, Glu 317, Thr 316, His 14, Glu 317, Arg 318, Met 16, Val 313, Leu 98, Lys 406
			S	N	Lys 100	H-acceptor	4.34	-1.3	
			6-ring	N	Arg 17	π-H	4.19	-0.7	

DS: Docking score energy (kcal.mol^{-1}); RMSD: Root-mean-square deviation (Å); L: Ligand; P: Protein; T: Type; D: Distance (Å); E: Energy (kcal.mol^{-1})

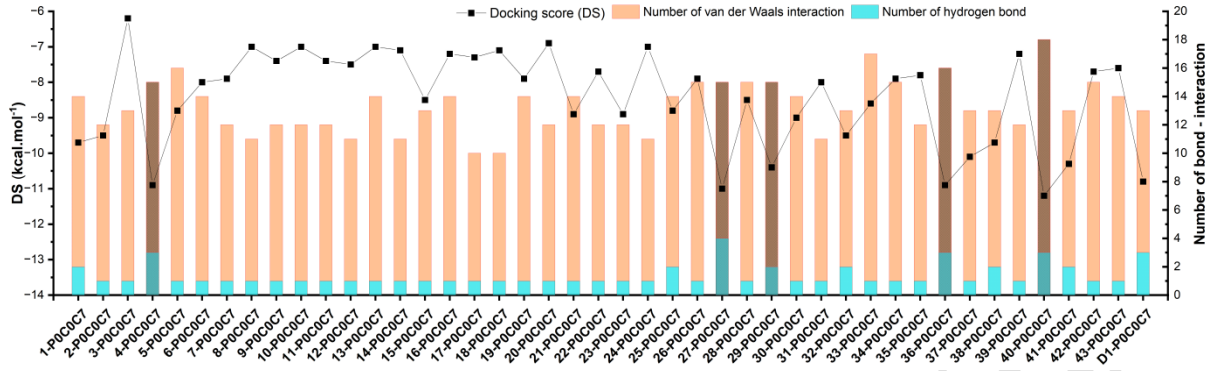

Fig. 6. Comparative analysis of the inhibitory docking score (DS) and the numbers of hydrogen bonds and van der Waals interactions for compounds **1–43** and the reference drug D1 with protein P0C0C7

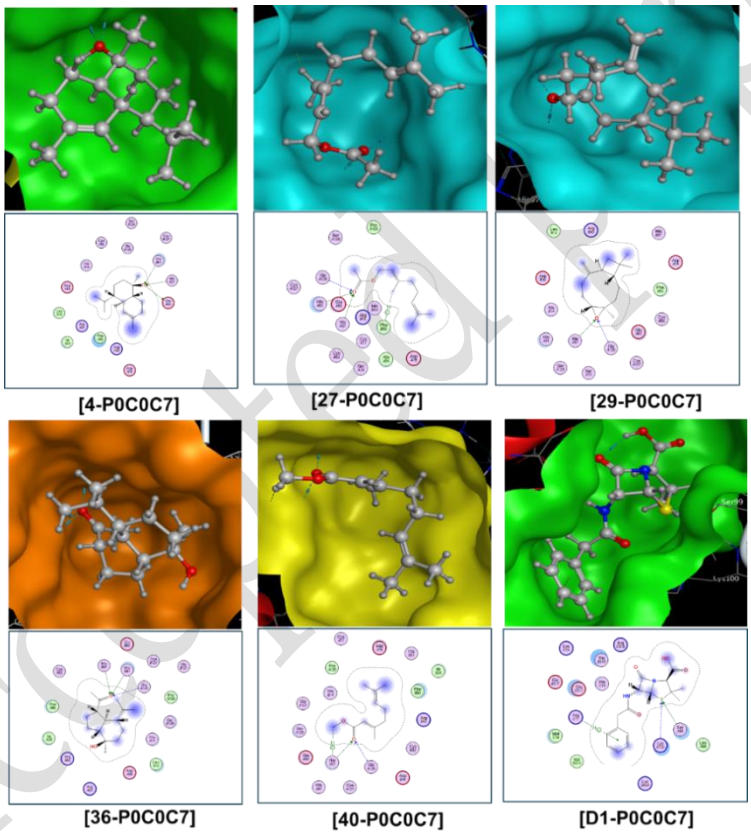

Fig. 7. Visual representations and binding pose interaction maps of the ligand–P0C0C7 complexes for the strongest predicted inhibitors

For the Q8DQF8 target, the docking results illustrated the inhibitory binding of the essential oil constituents and the reference drug (**D1**). The DS values, together with the associated hydrogen-bond and van der Waals interactions, account for the inhibition of protein Q8DQF8 (Fig. 6). The docking results revealed a broad distribution of binding affinities, with DS values ranging from -11.6 to -5.7 kcal.mol^{-1}, accompanied by 0–4 hydrogen bonds and 7–18 van der Waals interactions. Among the essential oil constituents (excluding **D1**), the most promising candidates were identified and ranked as **27–Q8DQF8** (-9.6 kcal.mol^{-1}) > **29–Q8DQF8** (-9.4 kcal.mol^{-1}) > **25–**

pISSN 1859-1388
eISSN 2615-9678

Q8DQF8 (-9.3 kcal.mol^{-1}) ≈ **41–Q8DQF8** (-9.3 kcal.mol^{-1}) > **36–Q8DQF8** (-9.2 kcal.mol^{-1}), which are highlighted in Fig. 8. The docking details and visualizations of the docking process for these compounds are shown in Table 3 and Fig. 9. In contrast, compound **14** was the weakest predicted inhibitor of Q8DQF8, with the least favorable docking score (DS = -5.7 kcal.mol^{-1}) and thus the lowest predicted binding strength among the screened ligands. The remaining compounds presented intermediate DS values (-6.0 to -9.1 kcal.mol^{-1}) associated with 0–1 hydrogen bonds and 7–12 van der Waals interactions, indicating that most compounds in this group do not bind to Q8DQF8 through hydrogen bonding. Instead, their binding is driven mainly by van der Waals interactions, which are generally weaker and less specific than hydrogen bonds are, resulting in less stable complexes and a reduced inhibitory potential. In addition, among the remaining compounds, **39** also presented a comparatively strong profile (DS = -9.2 kcal.mol^{-1}) and can be considered an additional candidate.

Table 3. Molecular docking simulation results of the ligand–Q8DQF8 complexes for the strongest predicted inhibitors

Ligand–protein			Hydrogen bond						van der Waals interaction
Name	DS	RMSD	L	P	T	D	E		
25–Q8DQF8	-9.3	1.0	O	O	Ser 48	H-donor	3.23	-0.6	Lys 47, Asp 169, Asn 52, Phe 96, Met 51, Pro 412, Leu 416, Ile 413, Phe 92, Phe 90
27–Q8DQF8	-9.6	1.27	O	N	Gln 94	H-acceptor	3.06	-1.5	Asn 52, Met 51, Asp 176, Ile 413, Ser 48, Asp 169, Phe 92, Ala 174, Pro 412, Leu 175, Gln 93
29–Q8DQF8	-9.4	1.46	O	N	Asn 52	H-acceptor	2.99	-2.6	Phe 90, Asp 169, Phe 92, Gln 94, Phe 96, Met 51, Ser 48, Pro 412, Leu 416, Ile 413
36–Q8DQF8	-9.2	1.56	O	O	Asp 49	H-donor	2.93	-2.7	Arg 208, Ser 53, Phe 278, Glu 205, Leu 217, Lys 52, Tyr 140, Ser 58, Tyr 112, Val 238, Thr 114
41–Q8DQF8	-9.3	0.75	O	N	Gln 94	H-acceptor	2.90	-3.7	Phe 90, Phe 96, Asn 52, Gln 93, Met 51, Ser 48, Phe 92, Asp 169
D1–Q8DQF8	-11.6	0.98	O	O	Asp 76	H-donor	2.80	-4.5	Ser 126, Cys 127, His 57, Gly 128, His 87, His 81, Ile 25, Cys 82, Arg 42, Arg 23, Phe 80, Leu 12, Asp 40, Cys 77, Glu 60, Ala 64, Ile 75, Ser 78
			O	N	Arg 68	H-acceptor	3.01	-3.5	
			O	N	Arg 68	H-acceptor	3.29	-0.8	
			6-ring	N	His 14	π-H	3.0	-0.6	

DS: Docking score energy (kcal.mol^{-1}); RMSD: Root-mean-square deviation (Å); L: Ligand; P: Protein; T: Type; D: Distance (Å); E: Energy (kcal.mol^{-1})

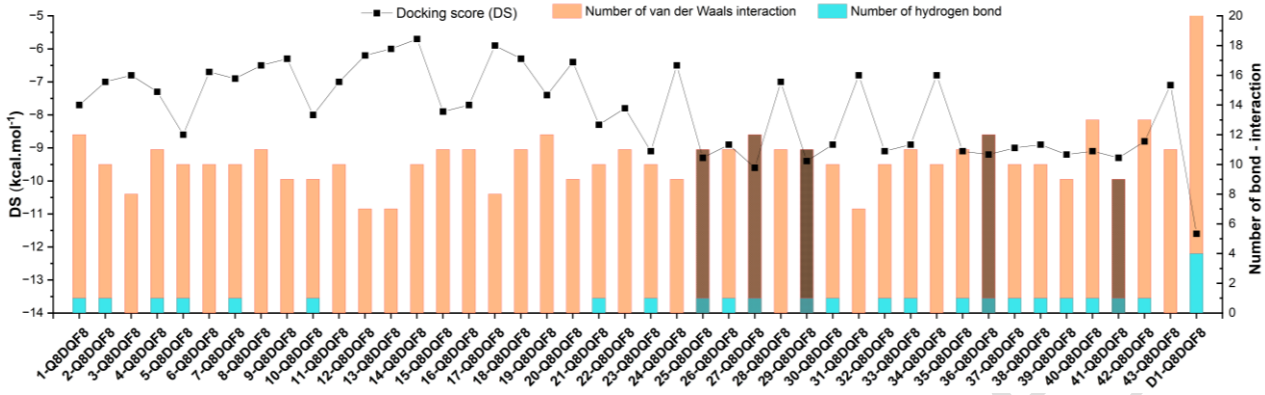

Fig. 8. Comparative analysis of the inhibitory docking score (DS) and the numbers of hydrogen bonds and van der Waals interactions for compounds **1–43** and the reference drug D1 with protein Q8DQF8.

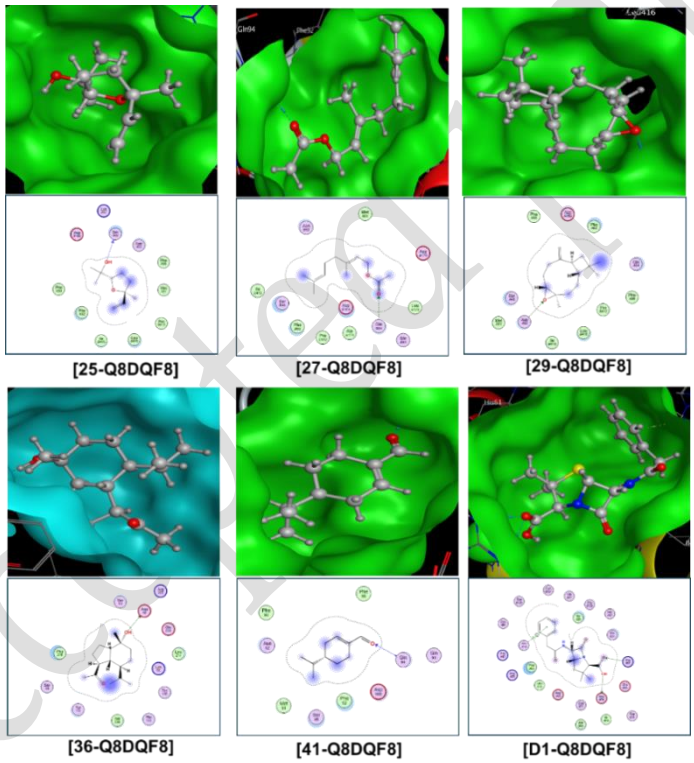

Fig. 9. Visual representations and binding pose interaction maps of the ligand–Q8DQF8 complexes for the strongest predicted inhibitors.

pISSN 1859-1388
eISSN 2615-9678

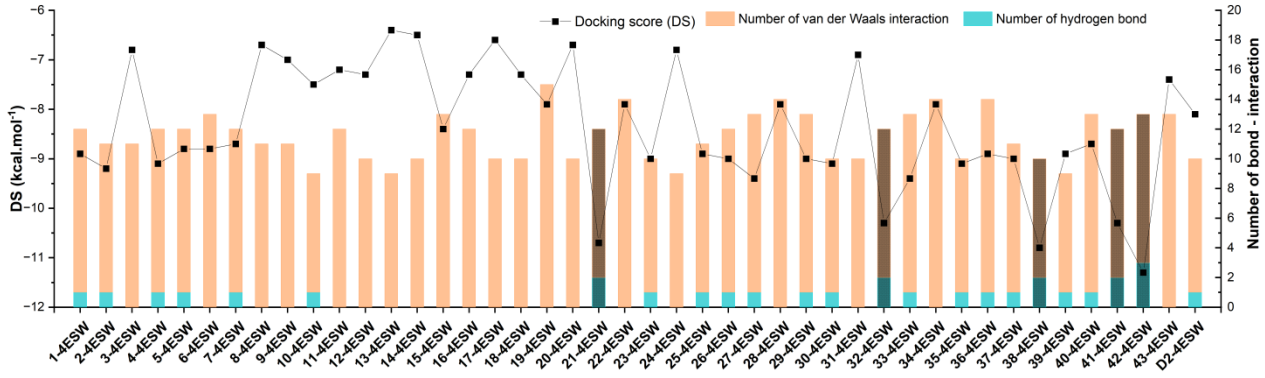

Fig. 10. Comparative analysis of the inhibitory docking score (DS) and the number of hydrogen bonds and van der Waals interactions for compounds **1–43** and the reference drug D2 with protein 4ESW.

Protein 4ESW was further examined to assess the binding of the reference drug clotrimazole. Figure 10 summarizes the docking scores (DSs) together with the numbers of hydrogen bonds and van der Waals interactions. Overall, the docking results revealed a wide range of binding affinities, with DS values from -11.3 to -6.4 kcal.mol^{-1}, accompanied by 0-3 hydrogen bond and 8-15 van der Waals interactions. A group of compounds with strong predicted inhibitory potential was identified and arranged in descending order of inhibitory activity as follows: **42–4ESW** (-11.3 kcal.mol^{-1}) > **38–4ESW** (-10.8 kcal.mol^{-1}) > **21–4ESW** (-10.7 kcal.mol^{-1}) > **32–4ESW** (-10.3 kcal.mol^{-1}) ≈ **41–4ESW** (-10.3 kcal.mol^{-1}), while detailed docking parameters and visualizations of the docking protein 4ESW are presented in Table 4 and Fig. 11**.** Compared with the reference drug (**D2**), these compounds in this group presented greater inhibitory activity than **D2** did (DS = -8.1 kcal.mol^{-1}), suggesting a greater ability to inhibit the protein under the current docking conditions. In contrast, compound **13** showed the weakest inhibitory ability, with DS = -6.4 kcal.mol^{-1}. The remaining groups presented intermediate DS values (approximately -7.0 to -9.4 kcal.mol^{-1} with 0–1 hydrogen bond and 8–13 van der Waals interactions).

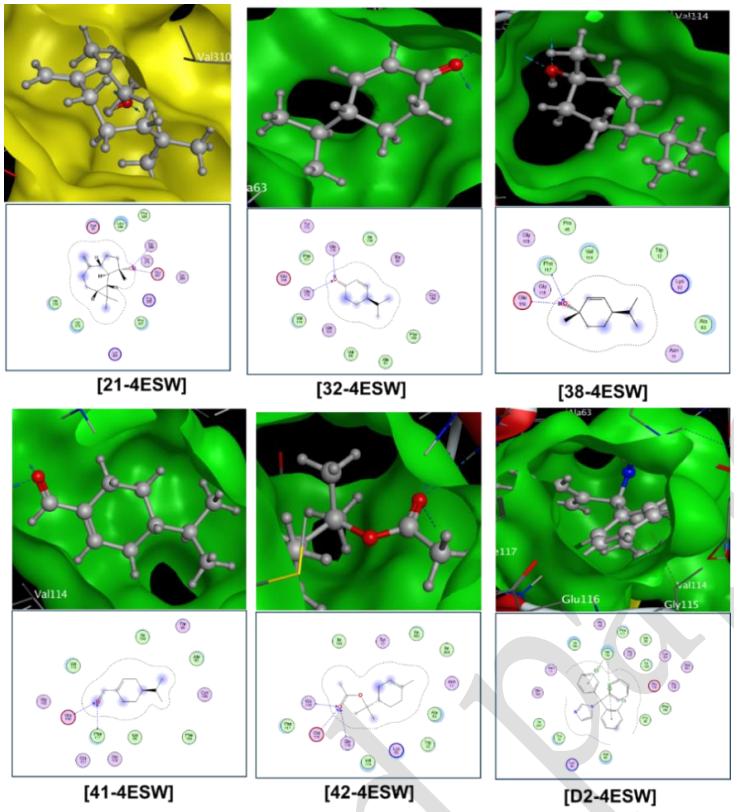

Fig. 11. Visual representations and binding pose interaction maps of the ligand–4ESW complexes for the strongest predicted inhibitors.

Table 4. Molecular docking simulation results of the ligand–4ESW complexes for the strongest predicted inhibitors.

Ligand–protein			Hydrogen bond						van der Waals interaction
Name	**DS**	**RMSD**	**L**	**P**		**T**	**D**	**E**	
21–4ESW	-10.7	1.68	O	N	Glu 267	H-acceptor	2.88	-1.6	Asp 85, Leu 338, Phe 265, Tyr 270, Ser 266, Arg 335, Pro 307, Lys 308, Val 272, Val 310
			O	N	Ser 268	H-acceptor	3.41	-0.8	
32–4ESW	-10.3	0.73	O	N	Gly 115	H-acceptor	3.03	-2.0	Tyr 113, Ile 158, Thr 89, Phe 198, Ala 63, Val 65, Gln 121, Val 114, Phe 117, Glu 116
			O	N	Gly 118	H-acceptor	2.97	-0.8	
38-4ESW	-10.8	1.01	O	N	Glu 116	H-acceptor	3.29	-0.8	Gly 118, Gly 115, Pro 45, Val 114, Trp 12, Lys 62, Ala 63, Asn 11
			O	N	Phe 117	H-acceptor	3.04	-2.2	
41–4ESW	-10.3	0.46	O	N	Glu 116	H-acceptor	3.01	-1.6	Gly 115, Val 114, Ile 158, Thr 89, Ala 63, Cys 199, Phe 198, Val 65, Gly 118, Gln 121
			O	N	Phe 117	H-acceptor	3.25	-0.7	
42–4ESW	-11.3	1.01	O	N	Gly 115	H-acceptor	3.36	-0.5	Phe 117, Ile 158, Tyr 17, Ile 160, Ile 201, Asn 11, Ala 63, Trp 12, Lys 62, Val 114
			O	N	Glu 116	H-acceptor	3.45	-1.3	
			O	N	Gly 118	H-acceptor	3.00	-2.3	
D2–4ESW	-8.1	0.46	5-ring	C	Arg 318	π-H	4.38	-0.6	Glu 317, Thr 316, Thr 319, Glu 317, Arg 320, Ser 98, Leu 98, Leu 97, His 14

DS: Docking score energy (kcal.mol^{-1}); RMSD: Root-mean-square deviation (Å); L: Ligand; P: Protein; T: Type; D: Distance (Å); E: Energy (kcal.mol^{-1})

pISSN 1859-1388
eISSN 2615-9678

Overall, the docking analysis results indicate that the most effective protein inhibitors among the identified constituents are oxygenated monoterpenes and oxygenated sesquiterpenes. These compounds typically contain functional groups such as hydroxyl, carbonyl, and epoxide groups, which enable the formation of hydrogen bonds while maintaining extensive van der Waals interactions through the nonpolar carbon backbone of terpenes. In contrast, other groups, including monoterpenes and sesquiterpene hydrocarbons, generally exhibited weaker binding affinities because of the absence of polar interactions between functional groups. Moreover, sesquiterpenoid structures with larger carbon backbones tended to exhibit enhanced inhibitory potential across P0C0C7, Q8DQF8, and 4ESW, suggesting that the size and architecture of the carbon skeleton are important factors influencing inhibitory activity.

Moreover, because the essential oil of *H. occulta* is a complex multicomponent system, the DS values obtained for individual compounds are insufficient to describe the inhibitory performance of the essential oil; thus, the constituent content of each compound should be considered. In this study, the major constituents linalool (40.35%), terpinen-4-ol (8.54%), and α-terpineol (3.05%) exhibited predominantly moderate DS values against the target proteins P0C0C7, Q8DQF8, and 4ESW from -6.5 to -8.5 kcal.mol^{-1}. The DS reflects the potential for molecular-level interactions, whereas the constituent content indicates the extent to which each component contributes within the mixture. Accordingly, major constituents such as linalool, terpinen-4-ol, and α-terpineol still have the potential to contribute to the evaluation of the inhibitory activity of *H. occulta* essential oils.

Physicochemical properties

The physicochemical parameters, including the average docking score (DS_{avg}, kcal.mol^{-1}), molecular weight (amu), polarizability (Å^3), molecular volume (Å^3), and lipophilicity/solubility descriptors (logP and logS) of the investigated compounds (**1–43**), are presented in Table 5. The pharmacokinetic potential of these compounds was assessed according to Lipinski's rule of five, a widely accepted criterion for predicting drug likeness.

The integration of physicochemical properties and the average docking score revealed that the investigated compounds exhibited excellent compliance with Lipinski's rule of five while simultaneously maintaining promising protein inhibitory potential. Notably, all 43/43 compounds presented molecular weights less than 500 amu, suggesting relatively small molecular sizes that are favorable for oral absorption. In addition, the number of hydrogen-bond donors and acceptors for these compounds were well below the rule-of-five thresholds, which may reduce excessive hydrogen bonding with the solvent and consequently support improved membrane permeability.

Regarding lipophilicity, the majority of the compounds presented LogP values ranging from approximately 2.5 – 4.8, demonstrating strong compliance with Lipinski's criterion (LogP < 5); only two compounds (15 and 43) slightly exceeded this threshold, indicating that the vast majority (**41/43**) maintained a reasonable balance between hydrophobicity and hydrophilicity. When correlated with the docking results, these candidates presented highly favorable docking scores ($DS_{avg} \leq$ -9.0 kcal.mol^{-1}) but also presented moderate logP values, not excessively low logS values, and low hydrogen-bonding capacities, suggesting that Lipinski-compliant physicochemical profiles not only support drug-likeness but also facilitate stable interactions

within the binding sites of the target proteins. When the docking data were compared, the subgroup displaying the most potent protein inhibition (lowest DS_{avg}) generally presented intermediate logP values, logS values within a suitable range and a low number of hydrogen bonds. This finding indicates that physicochemical properties aligned with Lipinski's rules not only support "drug-likeness" but can also structurally facilitate stable binding interactions with the target protein. Consequently, these compounds are considered promising candidates for future drug development.

Table 5. Physicochemical properties of the studied compounds (**1 - 43)**

Compound	DS_{avg} (kcal.mol^{-1})	Volume (Å^3)	Mass (amu)	Polarizability(Å^3)	Dispersion coefficients		Hydrogen-bond count P0C0C7/Q8DQF8/4ESW
					LogP	LogS	
1	-8.8	185.0	154.1	19.40	2.512	-1.806	2/1/1
2	-8.6	179.1	154.1	18.79	2.508	-1.753	1/1/1
3	-6.6	161.8	136.1	17.48	4.623	-4.671	1/0/0
4	-9.1	257.0	222.2	27.27	3.736	-2.945	3/1/1
5	-8.7	257.0	222.2	27.27	4.151	-3.422	1/1/1
6	-7.8	245.6	204.2	26.49	4.473	-4.316	1/0/0
7	-7.8	179.1	154.1	18.79	2.968	-2.043	1/1/1
8	-6.7	167.7	136.1	18.02	4.173	-4.068	1/0/0
9	-6.9	167.7	136.1	18.02	4.431	-4.033	1/0/0
10	-7.5	165.1	134.1	17.82	4.347	-3.916	1/1/1
11	-7.2	222.4	190.2	24.12	4.818	-5.151	1/0/0
12	-7.0	167.7	136.1	18.02	3.873	-3.673	1/0/0
13	-6.5	167.7	136.1	18.02	4.169	-3.932	1/0/0
14	-6.4	173.6	136.1	18.57	4.374	-4.152	1/0/0
15	-8.3	251.5	204.2	27.03	5.038	-5.215	1/0/0
16	-7.4	245.6	204.2	26.49	4.389	-4.286	1/0/0
17	-6.6	161.8	136.1	17.48	4.514	-4.408	1/0/0
18	-6.9	167.7	136.1	18.02	4.481	-4.259	1/0/0
19	-7.7	251.5	204.2	27.03	4.617	-4.474	1/0/0
20	-6.7	161.8	136.1	17.48	3.928	-3.816	1/0/0
21	-9.3	248.5	220.2	26.54	3.696	-3.700	1/1/2
22	-7.8	245.6	204.2	26.49	4.27	-4.300	1/0/0
23	-9.0	185.0	154.1	19.32	3.428	-2.954	1/1/1
24	-6.8	161.8	136.1	17.48	3.544	-3.730	1/0/0
25	-9.0	187.9	170.1	19.40	1.361	-0.710	2/1/1
26	-8.6	185.0	154.1	19.32	3.534	-3.075	1/1/1

pISSN 1859-1388
eISSN 2615-9678

Compound	DS_{avg} (kcal.mol^{-1})	Volume (Å^3)	Mass (amu)	Polarizability(Å^3)	Dispersion coefficients		Hydrogen-bond count P0C0C7/Q8DQF8/4ESW
					LogP	LogS	
27	-10.0	225.8	196.2	23.05	3.816	-3.329	4/1/1
28	-7.8	245.6	204.2	26.49	4.461	-4.279	1/0/0
29	-9.6	248.5	220.2	26.54	3.024	-2.915	2/1/1
30	-9.0	251.1	222.2	26.75	4.293	-3.902	1/1/1
31	-7.2	161.8	136.1	17.48	4.271	-4.163	1/0/0
32	-9.6	159.2	138.1	16.42	2.533	-2.070	2/1/2
33	-9.0	225.8	196.2	23.05	3.999	-3.510	1/1/1
34	-7.5	245.6	204.2	26.49	4.67	-4.761	1/0/0
35	-8.7	176.5	152.1	18.58	2.325	-1.620	1/1/1
36	-9.7	265.8	238.2	27.55	2.566	-2.306	3/1/1
37	-9.4	176.5	152.1	18.26	2.804	-2.374	1/1/1
38	-9.8	179.1	154.1	18.79	2.779	-1.864	2/1/2
39	-8.4	173.8	150.1	18.04	2.427	-2.135	1/1/1
40	-9.7	208.5	182.1	21.21	3.409	-3.168	3/1/1
41	-10.0	176.5	152.1	18.26	2.979	-2.373	2/1/2
42	-9.3	219.9	196.2	22.54	3.341	-2.876	1/1/3
43	-7.4	239.7	204.2	25.96	5.438	-5.564	1/0/0

ADMET prediction

The pharmacokinetic-toxicity properties of the investigated compounds, including absorption, distribution, metabolism, excretion, and toxicity (ADMET), were predicted, and the results are shown in Tables S4-S7. Most *H. occulta* essential oil constituents showed favorable absorption, with high Caco-2 permeability (logPapp 1.3 - 1.6) and high predicted human intestinal absorption (>92%), outperforming the two reference drugs (**D1, D2**). However, the investigated compounds exhibited low aqueous solubilities, with logS values ranging from approximately -2.0 to below -6.4, reflecting the lipophilic characteristics typical of essential oils. For dermal delivery, most compounds displayed relatively favorable skin permeation (logKp −1.0 to −2.4). In addition, most were not predicted to be P-glycoprotein substrates or inhibitors (P-gp I/II), suggesting a potentially lower risk of P-gp–mediated limitations on oral bioavailability or tissue penetration.

The investigated compounds exhibited logVDss values of 0.1 – 0.8, consistent with a moderate-to-high propensity for tissue distribution. Most constituents showed positive logBB values (approximately 0.3–0.8), indicating relatively good blood–brain barrier (BBB) permeability, which is generally higher than **D1** (-0.864) and only slightly lower than **D2** (0.938). In addition, the predicted central nervous system (CNS) permeability showed logPS values ranging from -1.4 to -2.8, which were lower than that of clotrimazole (-1.208) but higher than that of penicillin G (-2.943), suggesting a moderate-to-low tendency to penetrate the CNS, depending on the individual compound. From a metabolic perspective, most of these compounds were not

predicted to be CYP2D6 substrates, and only a few were predicted to be CYP3A4 substrates. Only a small number of compounds were predicted to inhibit major CYP enzymes (CYP1A2, CYP2C19, CYP2C9, CYP2D6, and CYP3A4). This suggests that the risk of metabolism-related drug–drug interactions is low.

On the excretion side, most compounds are predicted to be efficiently eliminated. They might not rely on OCT2-mediated renal transport, contributing to favorable pharmacokinetics. In addition, the lack of OCT2 inhibition suggests a low risk of drug–drug interactions and stable clearance. On the basis of the *in silico* toxicity assessment, most compounds in essential oils were Ames negative, showed no inhibition of hERG I/II channels, and were not predicted to be hepatotoxic. The estimated acute and chronic oral toxicity parameters (LD_{50} and LOAEL) were generally within an acceptable range. However, a notable limitation of this compound set is the relatively high prediction rate of skin sensitization, which should be considered when developing topical formulations, especially for long-term use.

4 Conclusion

In the present study, *Homalomena occulta* essential oil obtained via steam distillation was comprehensively profiled via GC–MS, resulting in the identification of 43 constituents. The oil composition was dominated by oxygenated monoterpenes, with linalool (40.35%), terpinen-4-ol (8.54%) and α-terpineol (3.05%) as the most abundant components, highlighting oxygenated terpenoids as the key chemical class. The identified compounds were then evaluated *in silico* via molecular docking simulations against three antimicrobial-related targets (P0C0C7, Q8DQF8, and 4ESW). The highest-ranking ligands were **40/27/4/36/29** for P0C0C7, **27/29/25/41/36** for Q8DQF8, and **42/38/21/32/41** for 4ESW. Docking results highlighted compounds **40** (Methyl geranate), **27** (Geranyl acetate), and **42** (α-Terpinyl acetate) as the top-ranked ligands for P0C0C7, Q8DQF8, and 4ESW, respectively, with compound 27 standing out for its strong ranking across multiple targets. In addition, a drug-likeness assessment based on Lipinski's rule of five suggested that the screened constituents largely fall within drug-like properties, as all the compounds met the molecular weight requirement (MW < 500 Da) and most satisfied the lipophilicity criterion (logP < 5; 41/43). ADMET profiling suggested generally good pharmacokinetic properties for the *H. occulta* essential oil compounds, with high predicted absorption and good permeability. The predictions also indicate a low risk of major transporter- and metabolism-related issues, supporting their suitability for further biological testing. Overall, these *in silico* findings provide a useful preliminary basis for prioritizing promising constituents and guiding subsequent experimental studies to evaluate their antimicrobial potential.

Acknowledgment

This work was supported by Hue University under the Core Research Program NCTB.DHH.2024.04; and the L'Oreal-UNESCO For Women in Science International Award 2023.

References

1. Fisher MC, Alastruey-Izquierdo A, Berman J, Bicanic T, Bignell EM, Bowyer P, et al. Tackling the emerging threat of antifungal resistance to human health. Nat Rev Microbiol. 2022;20(9):557–71.
2. Murray CJL, Ikuta KS, Sharara F, Swetschinski L, Aguilar GR, Gray A, et al. Global burden of bacterial antimicrobial resistance in 2019: a systematic analysis. Lancet. 2022;399(10325):629–55.

pISSN 1859-1388
eISSN 2615-9678

3. Poudel AN, Zhu S, Cooper N, Little P, Tarrant C, Hickman M, et al. The economic burden of antibiotic resistance: A systematic review and meta-analysis. PLoS One. 2023;18(5):e0285170.

4. Mitri EA, Reynolds GK, Copaescu AM, Cox F, Waldron JL, Peter JG, et al. State-of-the-Art Review: Antibiotic Allergy—A Multidisciplinary Approach to Delabeling. Clin Infect Dis. 2025;81(4):e74–92.

5. Atanasov AG, Zotchev SB, Dirsch VM, Supuran CT. Natural products in drug discovery: advances and opportunities. Nat Rev Drug Discov. 2021;20(3):200–16.

6. Swamy MK, Akhtar MS, Sinniah UR. Antimicrobial properties of plant essential oils against human pathogens and their mode of action: an updated review. Evidence-Based Complement Altern Med. 2016;2016(1):3012462.

7. Chouhan S, Sharma K, Guleria S. Antimicrobial activity of some essential oils—present status and future perspectives. Medicines. 2017;4(3):58.

8. Nazzaro F, Fratianni F, Coppola R, De Feo V. Essential oils and antifungal activity. Pharmaceuticals. 2017;10(4):86.

9. Man A, Santacroce L, Iacob R, Mare A, Man L. Antimicrobial activity of six essential oils against a group of human pathogens: A comparative study. Pathogens. 2019;8(1):15.

10. Sao Mai Dam HT Van. Chemical profiles and biological activities of essential oils of Arisaema and Homalomena species (Araceae)–A. J Phytol. 2022;14:41–9.

11. Ngan TTK, Hien TT, Tien LX, Toan TQ. Chemical compositions and stability of Vietnamese Homalomena occulta essential oil under the influence of storage conditions. Egypt J Chem. 2022;65(7):23–31.

12. Le Thuy T, Le Lam S, Van DN, Xuan AVH, Quang MN, Thanh MT, et al. In vitro antioxidant activity and content of bioactive compounds from Homalomena occulta. Hue Univ J Sci Nat Sci. 2024;133(1B):79–87.

13. Troeger C, Forouzanfar M, Rao PC, Khalil I, Brown A, Swartz S, et al. Estimates of the global, regional, and national morbidity, mortality, and etiologies of lower respiratory tract infections in 195 countries: a systematic analysis for the Global Burden of Disease Study 2015. Lancet Infect Dis [Internet]. 2017 Nov 1;17(11):1133–61. Available from: https://doi.org/10.1016/S1473-3099(17)30396-1

14. Havlickova B, Czaika VA, Friedrich M. Epidemiological trends in skin mycoses worldwide. Mycoses [Internet]. 2008;51(s4):2–15. Available from: https://onlinelibrary.wiley.com/doi/abs/10.1111/j.1439-0507.2008.01606.x

15. Kadioglu A, Weiser JN, Paton JC, Andrew PW. The role of *Streptococcus pneumoniae* virulence factors in host respiratory colonization and disease. Nat Rev Microbiol. 2008;6(4):288–301.

16. Silva-Costa C, Friaes A, Ramirez M, Melo-Cristino J. Macrolide-resistant *Streptococcus pyogenes*: prevalence and treatment strategies. Expert Rev Anti Infect Ther. 2015;13(5):615–28.

17. Fiedler T, Köller T, Kreikemeyer B. *Streptococcus pyogenes* biofilms—formation, biology, and clinical relevance. Front Cell Infect Microbiol. 2015;5:15.

18. Garvey MI, Baylay AJ, Wong RL, Piddock LJ V. Overexpression of patA and patB, which encode ABC transporters, is associated with fluoroquinolone resistance in clinical isolates of *Streptococcus pneumoniae*. Antimicrob Agents Chemother. 2011;55(1):190–6.

19. Mayer FL, Wilson D, Hube B. *Candida albicans* pathogenicity mechanisms. Virulence. 2013;4(2):119–28.

20. Lai RY, Huang S, Fenwick MK, Hazra A, Zhang Y, Rajashankar K, et al. Thiamin pyrimidine biosynthesis in *Candida albicans*: a remarkable reaction between histidine and pyridoxal phosphate. J Am Chem Soc. 2012;134(22):9157–9.

21. Babu TMC, Rajesh SS, Bhaskar BV, Devi S, Rammohan A, Sivaraman T, et al. Molecular docking, molecular dynamics simulation, biological evaluation and 2D QSAR analysis of flavonoids from Syzygium alternifolium as potent anti-*Helicobacter pylori* agents. RSC Adv. 2017;7(30):18277–92.

22. Tarasova O, Poroikov V, Veselovsky A. Molecular docking studies of HIV-1 resistance to reverse transcriptase inhibitors: Mini-review. Molecules. 2018;23(5):1233.

23. Thai KM, Le DP, Tran NVK, Nguyen TTH, Tran TD, Le MT. Computational assay of Zanamivir binding affinity with original and mutant influenza neuraminidase 9 using molecular docking. J Theor Biol. 2015;385:31–9.

24. Lipinski CA, Lombardo F, Dominy BW, Feeney PJ. Experimental and computational approaches to estimate solubility and permeability in drug

discovery and development settings. Adv Drug Deliv Rev. 1997;23:3–25.

25. Pires DEV, Blundell TL, Ascher DB. pkCSM: Predicting small-molecule pharmacokinetic and toxicity properties using graph-based signatures. J Med Chem. 2015;58(9):4066–72.